9980 *Biochemistry* **2009,** *48,* 9980–9993
DOI: 10.1021/bi9012897

BIOCHEMISTRY
including biophysical chemistry & molecular biology
Article

Strong Hydrogen Bond between Glutamic Acid 46 and Chromophore Leads to the Intermediate Spectral Form and Excited State Proton Transfer in the Y42F Mutant of the Photoreceptor Photoactive Yellow Protein[†]

Chandra P. Joshi,[‡] Harald Otto,[‡] Daniel Hoersch,[‡] Terry E. Meyer,[§] Michael A. Cusanovich,[§] and Maarten P. Heyn*[,‡]

[‡]*Biophysics Group, Department of Physics, Freie Universität Berlin, Arnimallee 14, 14195 Berlin, Germany, and* [§]*Department of Chemistry and Biochemistry, University of Arizona, Tucson, Arizona 85721*

Received July 27, 2009; Revised Manuscript Received September 18, 2009

ABSTRACT: In the Y42F mutant of photoactive yellow protein (PYP) the photoreceptor is in an equilibrium between two dark states, the yellow and intermediate spectral forms, absorbing at 457 and 390 nm, respectively. The nature of this equilibrium and the light-induced protonation and structural changes in the two spectral forms were characterized by transient absorption, fluorescence, FTIR, and pH indicator dye experiments. In the yellow form, the oxygen of the deprotonated *p*-hydroxycinnamoyl chromophore is linked by a strong low-barrier hydrogen bond to the protonated carboxyl group of Glu46 and by a weaker one to Thr50. Using FTIR, we find that the band due to the carbonyl of the protonated side chain of Glu46 is shifted from 1736 cm^{-1} in wild type to 1724 cm^{-1} in the yellow form of Y42F, implying a stronger hydrogen bond with the deprotonated chromophore in Y42F. The FTIR data suggest moreover that in the intermediate spectral form the chromophore is protonated and Glu46 deprotonated. Flash spectroscopy (50 ns−10 s) shows that the photocycles of the two forms are essentially the same except for a transition around 5 μs that has opposite signs in the two forms and is due to the chemical relaxation between the two dark states. The two cycles are coupled, likely by excited state proton transfer. The Y42F cycle differs from wild type by the occurrence of a new intermediate with protonated chromophore between the usual I_1 and I_2 intermediates which we call I_1H (370 nm). Transient fluorescence measurements indicate that in I_1H the chromophore retains the orientation it had in I_1. Transient proton uptake occurs with a time constant of 230 μs and a stoichiometry of 1. No proton uptake was associated however with the formation of the I_1H intermediate and the relaxation of the yellow/intermediate equilibrium. These protonation changes of the chromophore thus occur intramolecularly. The chromophore−Glu46 hydrogen bond in Y42F is shorter than in wild type, since the adjacent chromophore−Y42 hydrogen bond is replaced by a longer one with Thr50. This facilitates proton transfer from Glu46 to the chromophore in the dark by lowering the barrier, leading to the protonation equilibrium and causing the rapid light-induced proton transfer which couples the cycles.

Photoactive yellow protein (PYP)[1] is a bacterial photoreceptor that is the structural prototype of the PAS domain family of signaling proteins. (*1*−*6*). It is a small globular cytoplasmic α/β protein (14 kDa) whose three-dimensional structure has been determined in both the dark state and some of its transient photointermediates (*7*−*9*). Absorption of light by its *p*-hydroxycinnamoyl chromophore (λ_{max} 446 nm) leads in about 3 ps to photoisomerization around the chromophore C_7=C_8 double bond (*10*, *11*). Isomerization is followed by a series of dark reactions on the nanosecond, microsecond, and millisecond time scales (*12*, *13*). The system returns to the initial dark state within 1 s. In the course of these dark relaxation reactions the initial structural perturbation of the chromophore is transmitted to the protein, leading on the millisecond time scale to a major structural change in the I_2' intermediate. This global structural change has been detected by solvent effects on the kinetics (*14*), NMR (*15*), CD (*16*, *17*), small-angle X-ray scattering (*18*), and FTIR (*19*, *20*). It has been characterized as a partial unfolding of the protein with the N-terminal cap dissociating from the central antiparallel β-sheet (*17*, *21*, *22*, *54*). Formation of I_2' is associated with the transient exposure of a hydrophobic surface patch (*14*, *23*). The longest lived intermediate I_2' is identified with the signaling state, although no interaction with a response regulator has been observed. The kinetics of the photocycle has been studied in detail by a variety of methods including transient absorption in the visible and UV (*12*, *13*, *24*, *54*), transient fluorescence (*25*), and time-resolved FTIR (*19*, *20*).

Due to the availability of high-resolution structural data both in the crystalline state and in solution, PYP has developed into a model system for PAS domain signaling proteins and for more general questions in biophysical chemistry such as protein folding (*21*, *26*) and hydrogen bonding (*27*−*30*).

[†]This work was supported by a grant from the Deutsche Forschungsgemeinschaft to M.P.H. and H.O. (He 1382/13-2).

*To whom correspondence should be addressed. E-mail: heyn@physik.fu-berlin.de. Phone: 0049-30-83856160. Fax: 0049-30-83856299.

[1]Abbreviations: PYP, photoactive yellow protein; FTIR, Fourier transform infrared; GFP, green fluorescence protein; BCP, bromocresol purple; PAS, acronym formed of the names of the first three proteins recognized as sharing this sensor motif (*p*eriodic clock protein of *Drosophila*, *a*ryl hydrocarbon receptor nuclear translocator of vertebrates, *s*ingle-minded protein of *Drosophila*); SVD, singular value decomposition; LBHB, low-barrier hydrogen bond; LED, light emitting diode; ESPT, excited state proton transfer; PR, photoreversal; CW, continuous wave.

 Published on Web 09/20/2009

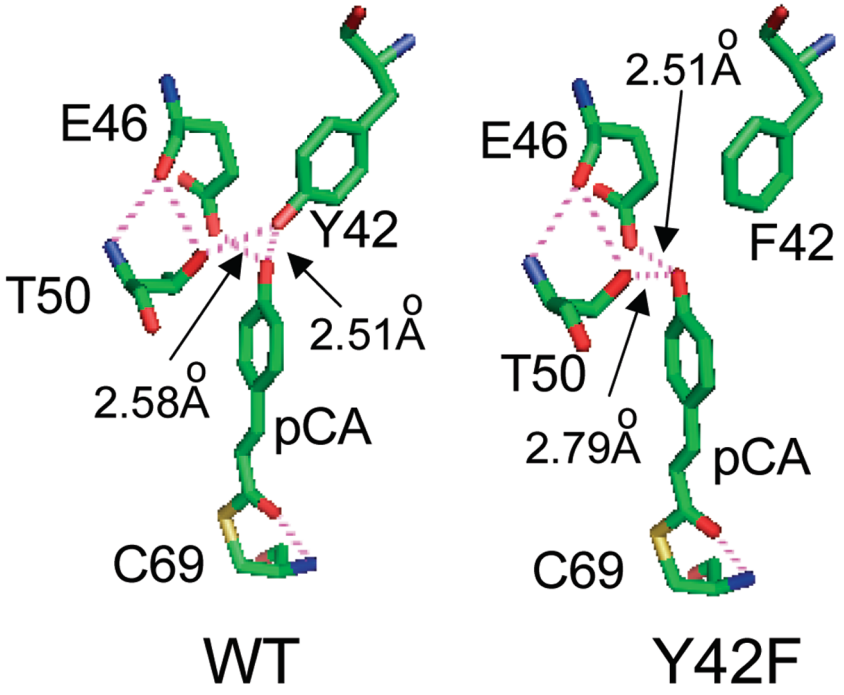

FIGURE 1: Structures of the active sites in wild type (left) and the yellow form of Y42F (right). The oxygen of the deprotonated chromophore is linked by a pair of bifurcated hydrogen bonds to E46 and Y42 in wild type and to E46 and T50 in Y42F. Carbon, oxygen, nitrogen, and sulfur atoms are shown in green, red, blue, and yellow, respectively. The pink dots indicate the hydrogen-bonding network. The lengths of the key hydrogen bonds are indicated and taken from refs *8* and *36*.

The chromophore of PYP is anchored in its binding pocket by three hydrogen bonds (see Figure 1, left). The carbonyl of the chromophore's thioester linkage is hydrogen bonded to the amino group of backbone residue 69. In the dark state, the oxygen of the deprotonated chromophore is hydrogen bonded to the protonated side chains of residues Y42 and E46 by a bifurcated pair of hydrogen bonds. These are still present after isomerization in the red-shifted I_1 intermediate (deprotonated chromophore, λ_{max} 460 nm), in which only the hydrogen bond with the backbone is broken (*31*), but are lost in the following I_2 and I_2' intermediates (absorbing in the UV at 370 and 350 nm, respectively (*48*, *13*)), in which the chromophore is protonated. The role of residue E46 has been intensively investigated (*19*, *20*, *32*−*34*). We focus here on the interplay between the two hydrogen bonds of the chromophore's oxygen with Y42 and E46.

The two hydrogen bonds of the chromophore with E46 and Y42 are unusually short and strong with O···O distances of 2.58 and 2.51 Å, respectively (*28*, *29*). Recently, direct information about the proton positions in these bonds was obtained for the first time from neutron diffraction (*27*). For the proton in the hydrogen bond between the chromophore and E46, the distances to the phenolic oxygen and the carboxylic oxygen were 1.37 and 1.21 Å, respectively (*27*). Since the average covalent O−H bond length is 0.95 Å, this indicates that this proton is not covalently bound to either oxygen but is essentially shared by the two oxygen atoms (*27*). This implies that the proton affinities of E46 and the chromophore in the dark are similar. It was concluded that this proton is in a low-barrier hydrogen bond (LBHB) (*27*). For the short hydrogen bond with Y42, on the other hand, the distances are very different. The distance between this proton and the phenolic oxygen of Y42 is 0.96 Å, close to the average O−H bond length, making this a covalent bond.

The role of active site residue Y42 and its hydrogen bond with the chromophore has been investigated in a number of studies. It was observed with the mutant Y42F that replacement of the short hydrogen bond between the chromophore and Y42 by one of normal length with T50 leads to the formation of a shoulder around 390 nm on the blue side of the absorption maximum (457 nm) (*35*−*37*) (see spectrum in Figure 8A). This spectral species is called the intermediate spectral form and is also observed in the Y42A and Y42W mutants (*35*−*38*). In these mutants, the dark state is in an equilibrium between the yellow (450−458 nm) and intermediate spectral (390 nm) forms. This equilibrium can be shifted in the direction of the intermediate spectral form by raising the temperature or by the addition of chaotropes (*36*, *38*). The Y42F mutant has reduced stability against denaturation (*36*, *38*); however, tyrosine 42 is not essential for the formation of the signaling state as Y42F has the same bell-shaped pH dependence of the photocycle recovery rate as wild type (*36*). The structure of the yellow form of the Y42F mutant (favored by the crystallization procedure) was determined by X-ray diffraction (*36*). The aromatic ring of the chromophore is moved by about 0.8 Å with respect to its wild-type position (see Figure 1). A new but weaker (2.79 Å) hydrogen bond of the chromophore with the OH group of T50 replaces the stronger hydrogen bond (2.51 Å) with Y42 present in wild type (*36*) (see Figure 1). The diffraction data show moreover that the distance between the oxygens of E46 and the chromophore is less in the mutant Y42F than in wild type (2.51 vs 2.58 Å) (*36*), making this an even stronger hydrogen bond. The structure of the intermediate spectral form is not available. It was concluded from UV resonance Raman experiments at 325 nm that the chromophore in the intermediate spectral form is protonated (*39*), correcting previous FT Raman measurements in which no selective excitation of the intermediate form was achieved (*36*). Ultrafast absorption measurements showed that, in the mutant Y42F, the formation of the I_1 intermediate, with deprotonated chromophore, is 100 times faster than in wild type (30 ps vs 3 ns) (*40*).

Photocycle measurements on the millisecond time scale indicated only the presence of a protonated intermediate absorbing in the UV (*36*, *37*). Interestingly, the fluorescence excitation spectrum had the shape of the absorption spectrum, i.e., included the shoulder at 390 nm due to the intermediate spectral form (*36*), although the fluorescence originates from the yellow form. Based on studies with a number of mutants, it was concluded that residue E46 and its hydrogen bond with the chromophore are prerequisites for the existence of the intermediate spectral form (*38*).

The goal of this study is to gain a better understanding of the nature and properties of the intermediate spectral form with particular emphasis on the role of the hydrogen bond between E46 and the chromophore. We suggest that replacement of the hydrogen bond of the chromophore's oxygen with Y42 by the weaker one with T50 in the mutant Y42F strengthens the chromophore's second hydrogen bond with E46. This increases the proton affinity of the chromophore in the Glu−chromophore hydrogen bond and lowers the barrier for proton transfer, facilitating intramolecular proton transfer via this hydrogen bond in the dark and leading to the equilibrium with the intermediate spectral form with protonated chromophore. Our observations indicate moreover that, in the intermediate spectral form, rapid light-induced proton transfer from the chromophore occurs, effectively coupling the photocycles of the two spectral forms.

MATERIALS AND METHODS

Protein Production and Purification. *Halorhodospira halophila* holo-PYP was produced by coexpression with the biosynthetic enzymes TAL and pCL and subsequently purified from *Escherichia coli* BL21(DE3) as described (*41*). The mutagenesis was also performed as described (*42*).

Transient Absorption Spectroscopy and Data Analysis. Time-resolved absorption spectroscopy with nanosecond time resolution by single and double flash excitation was performed as described (*23*, *43*−*45*). Amplitude spectra were determined from the transient absorbance data using singular value decomposition methods as described previously (*13*, *23*, *24*, *46*, *47*). Matrix calculations including singular value decomposition were performed with Matlab version R 12.1. Fits with sums of exponentials were carried out with Microcal Origin version 7.5.

Kinetics of Bulk Protonation Changes and Dye Binding. Light-induced proton release and uptake were monitored using the pH indicator dye BCP in unbuffered solution as described (*23*). The proton uptake stoichiometry was determined as described (*23*, *33*). Measurements of the kinetics of dye binding were performed with the same dye in the presence of 30 mM Tris. Titrations were carried out by adding microliter aliquots of 10−100 mM HCl or KOH.

Transient Fluorescence Spectroscopy. Time-resolved fluorescence spectroscopy was performed as described (*25*).

Simultaneous Measurement of UV−*Vis and FTIR Spectra*. FTIR spectra were recorded using a Nicolet 20 SXB Fourier transform infrared spectrometer. A UV−vis fiber-optic spectrometer was incorporated into this FTIR spectrometer as shown in Supporting Information Figure S1, allowing the simultaneous measurement of FTIR and optical spectra of the same sample. Moreover, a CW laser emitting at 475 nm provided background illumination producing a photostationary state and allowing the measurement of light minus dark difference spectra.

The sample cell consisted of two CaF_2 windows (25 mm diameter, 2 mm thickness) separated by an annular spacer (6 μm; Trespaphan, Hoechst). One microliter of 10 mM Tris at pH 7 was placed at the center of one of the plates and a few microliters of concentrated PYP at pH 7 was added. The sandwich consisting of the two plates and the spacer was closed quickly, and vacuum grease (Bayer silicone paste; Bayer AG) was applied to the edge of the plates to prevent evaporation.

The sample and reference cells were mounted in a homemade sample holder. The reference cell consisted of two empty CaF_2 plates separated by a 19 μm spacer. This was used to measure the absolute FTIR and optical spectra. The sample and reference cell were each placed between two rubber rings, fitted in the corresponding grooves of the sample holder, and fixed by an additional cover plate (with suitable holes in it) using screws. Visual inspection showed that the yellow sample was distributed homogeneously over the plates. The sample holder was positioned vertically using a supporting base and an additional plate in such a way that the sample holder can be moved up and down via a computer-controlled motor to place either the sample or the reference cell in the IR beam. This supporting base can be rotated around the vertical axis to tilt the sample cell (in this case 45° with respect to the IR radiation) so that the other two beams (the laser for the bleach and the measuring beam of the fiber-optic spectrometer) also cross at the same area of the sample; see Supporting Information Figure S1. The laser beam at 475 nm (30 mW; Roithner Lasertechnik, Austria; beam expanded with a lens) was incident at an angle of about 90° to bleach the sample. The absorption spectra were measured using fiber optics with a UV−vis NIR light source (Mikropack, DT-Mini-2-GS) and a CCD detector (avantes, Avaspec-2048). The measuring light of the fiber-optic spectrometer was aligned at an angle of about 45° with respect to the sample plate. The temperature of the sample was controlled with a thermostat (Julabo Labortechnik GmbH, Germany) and was measured at a position very close to the sample cell.

Both absolute and light minus dark difference FTIR and optical spectra were measured. Depending on the spectrum measured, either the empty plates or the sample itself in the dark state served as the reference.

RESULTS

Photocycles of the Yellow and Intermediate Spectral Forms, Transient Absorbance. The photocycle of the yellow form was measured at pH 7 with excitation at 460 nm. Transient absorbance data were acquired at 18 wavelengths from 340 to 510 nm. Selected time traces at 6 diagnostic wavelengths are shown in Figure 2A. To investigate the photocycle of the intermediate spectral form, a similar data set was collected with excitation at 355 nm. These data are presented in Figure 3A. From a comparison of the two data sets, it is apparent that they contain similar if not identical time constants. Therefore, both data sets were subjected to a combined singular value decomposition analysis in the time range from 100 ns to 10 s. The number of significant singular values was four, suggesting contributions from four species during the cycle. It will be shown that these are the intermediates I_1H, I_2, I_2', and the dark state of the intermediate form P^{390}. The unweighted basis vectors of the time traces from the SVD analysis could be fitted with a sum of four exponentials also indicating the same number of transitions. The corresponding time constants τ_1 = 5 μs, τ_2 = 65 μs,

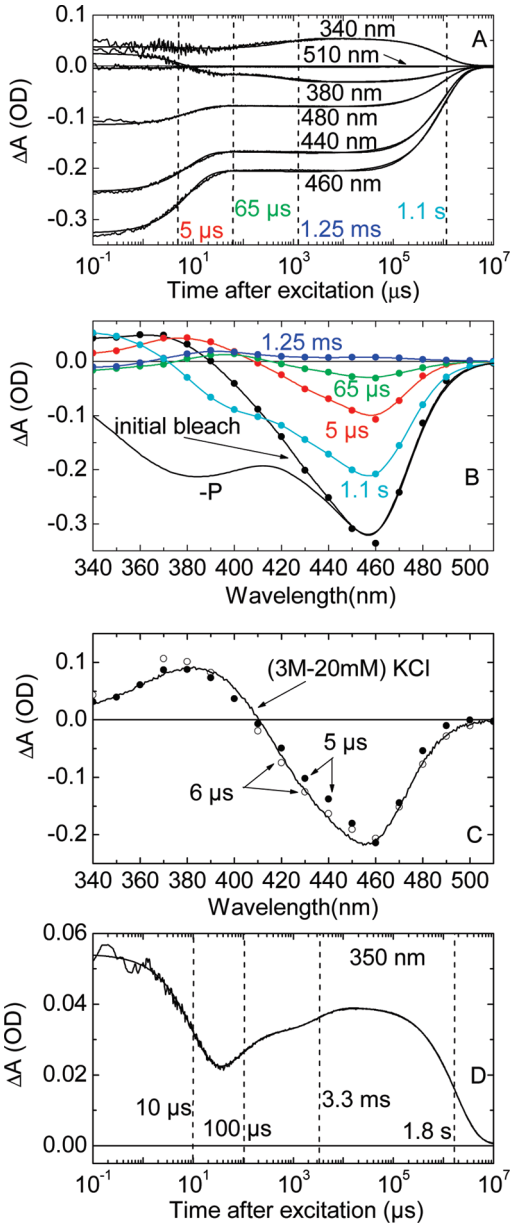

FIGURE 2: (A) Transient absorption changes after excitation at 460 nm at 6 selected wavelengths (out of a total of 18 varying from 340 to 510 nm in steps of 10 nm). This data set and the corresponding one with excitation at 355 nm (presented in Figure 3A) were subjected to combined singular value decomposition, as described in the text. The four vertical dashed lines indicate the time constants from a global fit of the combined data sets with a sum of four exponentials. The solid lines are the fits. Conditions: 50 mM KCl, 50 mM Tris, pH 7, 21 °C, path length 5 mm. Absorption at 457 and 385 nm of the ground-state spectrum was 0.85 and 0.57 OD, respectively. (B) Amplitude spectra calculated as described in the text. The four amplitude spectra correspond to the time constants $\tau_1 = 5\ \mu s$ (red), $\tau_2 = 65\ \mu s$ (green), $\tau_3 = 1.25$ ms (blue), and $\tau_4 = 1.1$ s (light blue). The curve with black circles is the sum of all four amplitude spectra and represents the initial bleach. The continuous curve (-P) is a scaled and inverted ground-state spectrum to fit the initial bleach in the wavelength range λ 440 nm. (C) Comparison of the 5 μs amplitude spectrum (black filled circles) from panel B (red filled circles, scaled up by a factor of 2) with the difference absorption spectrum between the yellow and intermediate spectral forms calculated as described in the text (continuous curve). Also shown is the 6 μs amplitude spectrum (open circles) calculated from the global fit of the data of Figure 3C. (D) Time trace of the transient absorption change at 350 nm with an LED as the measuring light. The solid line is a fit of this curve with a sum of four exponentials. The four vertical dashed lines indicate the time constants from this fit.

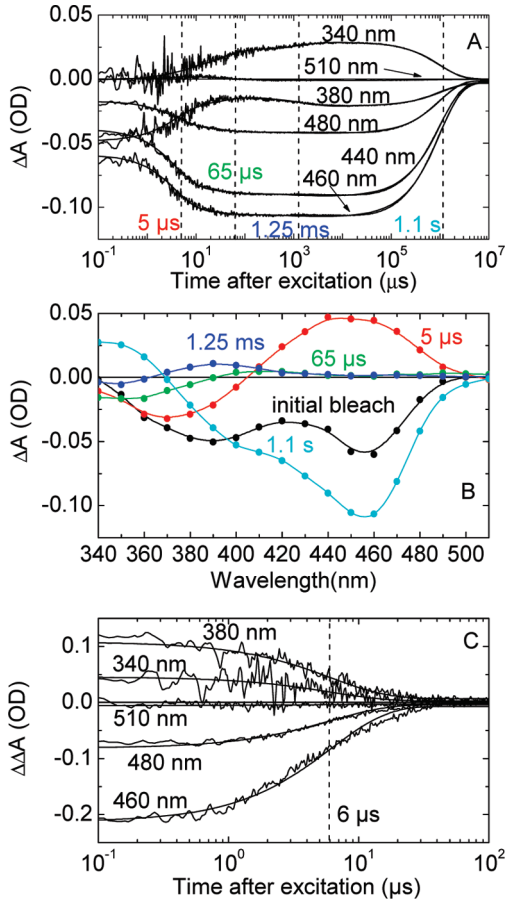

FIGURE 3: (A) Transient absorption changes of the same sample used in Figure 2A following excitation at 355 nm at 6 selected wavelengths. Measurements were carried out at the same 18 wavelengths as in Figure 2A. This data set and the 460 nm excitation data (Figure 2A) were subjected to combined singular value decomposition. The vertical dashed lines correspond to the time constants from the global fit. The solid lines are the fits with a sum of four exponentials. (B) The four amplitude spectra correspond to the time constants $\tau_1 = 5\ \mu s$ (red), $\tau_2 = 65\ \mu s$ (green), $\tau_3 = 1.25$ ms (blue), and $\tau_4 = 1.1$ s (light blue). The sum of the four amplitude spectra is the initial bleach and is shown as the curve with black circles. (C) Differences between the transient absorbance changes measured using the 460 and 355 nm excitation at five selected wavelengths. The 355 nm excitation data set is scaled up by a common factor of 1.9. A global fit of the traces at all 18 wavelengths with a single exponential results in a time constant of 6 μs, as indicated by the vertical dashed line. The solid lines are the fits.

$\tau_3 = 1.25$ ms, and $\tau_4 = 1.1$ s of the fit are indicated by the dashed vertical lines in Figures 2A and 3A. Also shown in these panels are the fit curves to the time traces. The amplitudes from the above fit and the weighted wavelength-dependent basis vectors were used to calculate the corresponding amplitude spectra as described (*43*, *46*, *24*). These amplitude spectra for excitation at 460 and 355 nm are presented in Figures 2B and 3B, respectively. At the beginning of data acquisition (at 100 ns after the flash) in Figure 2A, there is positive absorbance between 340 and 380 nm suggesting the presence of a species with protonated chromophore. The trace at 510 nm has negligible amplitude indicating the absence of a red-shifted I_1 intermediate on the time scale investigated. The 5 μs component in Figure 2A,B is of large amplitude and corresponds to a transition from a species absorbing around 380−390 nm to the 457 nm yellow form. We suggest that this transition is due to the relaxation of the ground-state equilibrium between the yellow and intermediate spectral

forms after depletion of the yellow ground state by the excitation flash at 460 nm. This would lead to an absorbance decrease in the UV and an increase around 460 nm, as observed in the amplitude spectrum for this component (Figure 2B). Further support for this proposal is provided by the following observations. KCl shifts the dark equilibrium between the yellow and intermediate spectral forms in the direction of the intermediate form (*36*, *38*). The difference spectrum for the interconversion of these forms was obtained by subtracting the UV−vis spectra at 3.0 and 0.02 M salt. As shown in Figure 2C, this difference spectrum fits quite well with the scaled 5 μs amplitude spectrum, in accordance with our hypothesis. Additional evidence comes from experiments with the kosmotrope $(NH_4)_2SO_4$. At 3 M $(NH_4)_2SO_4$ and pH 7 the equilibrium is almost completely on the side of the yellow form (*36*). In the absence of the intermediate spectral form, no relaxation can occur when the yellow form is depleted by flash excitation. Under these conditions, the 5 μs transition was absent in the photocycle time traces (data not shown), in agreement with our hypothesis.

The next two transitions, at 65 μs and 1.25 ms, are of small amplitude and involve intermediates absorbing in the UV. The amplitude spectrum indicates a blue shift for the 1.25 ms component, which represents the formation of the I_2' intermediate. Since the traces for the UV wavelengths in Figure 2A are of small amplitude and rather noisy, we present in Figure 2D data at 350 nm obtained with an intense LED emitting at 350 nm as the measuring light source. This allows acquisition of data of higher signal-to-noise ratio and shows more clearly the initial presence of a UV-absorbing intermediate and the microsecond relaxation followed by two transitions around 100 μs and 3.3 ms. The initial bleach of Figure 2B, the sum of the amplitude spectra, also shows the presence of a species with protonated chromophore absorbing in the UV at the beginning of data collection and moreover confirms the absence of an I_1-like photocycle intermediate with deprotonated chromophore which would show up as a positive difference absorbance near 500 nm (*13*). The initial bleach thus differs in a major way from that of wild type, which is characterized by a red-shifted I_1 intermediate and the absence of an intermediate absorbing in the UV (*13*). The I_1 intermediate of wild type seems to be replaced by a UV-absorbing intermediate in the mutant Y42F in the time range investigated.

The photocycle of the intermediate spectral form was measured at pH 7 with excitation at 355 nm with the same sample that was used to collect the data of Figure 2 with 460 nm excitation. Data were again taken at 18 wavelengths. The results at the same 6 wavelengths as in Figure 2A are shown in Figure 3A. The data are noisier due to a lower fraction of cycling molecules in the intermediate spectral form. Apart from the sign of the first microsecond transition, the time traces are strikingly similar to those of the yellow form in Figure 2A. The reversed sign of the amplitude of the first component is in perfect agreement with our tentative interpretation of this component as the relaxation of the dark equilibrium. In this case, the intermediate spectral form is depleted by the 355 nm flash, and the ground-state equilibrium shifts from the yellow toward the intermediate spectral form. Therefore, the absorbance should decrease around 460 nm and increase near 380 nm as observed. Moreover, the relaxation time should be the same whether the yellow or intermediate form is depleted, since the relaxation rate is the sum of the forward and backward rate constants. The equality of the microsecond times and the sign reversal of its amplitude thus strongly support our interpretation.

Amplitude spectra are shown in Figure 3B. The amplitude spectrum for the 5 μs component clearly shows that this is a transition from the yellow ground state to the intermediate spectral form. The 65 μs and 1.25 ms components correspond again to blue shifts indicating the formation of the I_2 and I_2' intermediates. The initial bleach shows, in addition to the expected depletion at 390 nm, also depletion at 460 nm. This is due to the fact that excitation at 355 nm also initiates the cycle of the yellow form by absorption in one of its higher excited states. The initial bleach shows that, around 100 ns, a UV-absorbing species is present. This is less clear than in the corresponding initial bleach spectrum of the yellow form due to the large negative contribution from the depletion of the intermediate spectral form. Again, there is no evidence for an I_1 photocycle intermediate in the time window from 100 ns to 10 s.

If our working hypothesis that the cycles of the two spectral forms are the same apart from the sign of the relaxation component is correct, subtracting the transient absorption data with excitation at 460 and 355 nm should result in just the microsecond component with no absorbance changes at later times. The results of such a test are shown in Figure 3C. Due to differences in extinction coefficient, quantum yield of cycling, etc., the data set at 355 nm was scaled up by a common factor of 1.9 at all 18 wavelengths. Five of these time traces at selected wavelengths are shown. Clearly, the absorbance change is zero beyond 30 μs as expected. A global fit at all wavelengths led to a single exponential decay with a time constant of 6 μs. The amplitude spectrum of this transition is shown in Figure 2C and fits well with the difference spectrum between the two spectral forms.

The data strongly suggest that the two cycles are coupled. Not only is there a rapid ground-state equilibrium between the two forms, but the cycle of the intermediate spectral form seems to merge with the yellow cycle well before our data acquisition starts around 100 ns, probably shortly after excitation.

Kinetics of the Photocycle from Transient Fluorescence. The results from transient absorption suggest the presence of three photocycle intermediates with protonated chromophore. The cycle of wild type has only two such intermediates, I_2 (370 nm) and I_2' (350 nm), in addition to the intermediate I_1 with deprotonated chromophore absorbing at 460 nm. To clarify the differences between these photocycle intermediates, we carried out transient fluorescence measurements, since such experiments are sensitive to the chromophore orientation (*25*). In these experiments, the transient fluorescence of tryptophan 119, the only tryptophan of PYP, is monitored (*25*, *48*). W119 is located on the antiparallel β-sheet that separates the PAS core from the N-terminal domain. The emission of W119 is quenched by energy transfer to the *p*-hydroxycinnamoyl chromophore (*48*). The rate of energy transfer is proportional to the product of the κ^2 factor, which depends on the orientations of donor and acceptor, and the spectral overlap J between donor emission and acceptor absorption spectra. In the course of the photocycle, both κ^2 and J change, leading to characteristic changes in the fluorescence lifetime of W119 (*25*, *48*). The κ^2 values are calculated from the X-ray structures of the intermediates. In transient fluorescence, the steady-state fluorescence of W119 is time-resolved. In Figure 4A, the transient absorbance at 350 nm is compared with the transient fluorescence for wild-type PYP. In I_1 (460 nm), the κ^2 factor is little changed with respect to the initial state, but the spectral overlap J is less than in the dark state (446 nm), leading

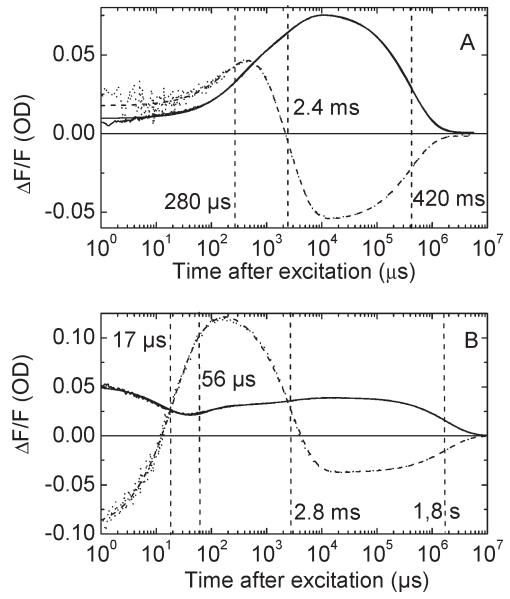

FIGURE 4: Comparison between the normalized transient fluorescence changes $\Delta F/F$ of tryptophan W119 (dotted line) and the transient absorption changes of the *p*-hydroxycinnamoyl chromophore (solid line) at 350 nm for wild-type PYP (A) and the Y42F mutant (B). Flash excitation at 460 nm. The time traces of panel A were fitted simultaneously with a sum of three exponentials and those of panel B with a sum of four exponentials. The solid and dashed lines are the fit curves for the transient absorption and fluorescence, respectively. The vertical dashed lines indicate the time constants of the fits. Conditions for (A) and (B): 20 °C, 300 mM KCl, 30 mM Tris, pH 7, path length 3 mm.

to a small increase in fluorescence (*25*) indicated by the initial positive $\Delta F/F$ of Figure 4A (dotted curve). In the I_1 (460 nm) to I_2 (370 nm) transition, the spectral overlap J increases, but simultaneously κ^2 decreases by a larger factor, leading to a substantial increase in fluorescence (*25*), indicated by the 280 μs transition in Figure 4A. In the I_2 to I_2' (350 nm) transition (2.4 ms), the overlap J barely changes, but there is a large decrease in fluorescence (*25*), probably caused by an increase in κ^2 or changes in the environment of W119. From the comparison between the time traces, it is clear that the transient fluorescence is much more sensitive than transient absorbance to transitions between the two similar UV-absorbing intermediates due its dependence on κ^2. The vertical lines in Figure 4A indicate the time constants of a simultaneous fit to the two signals.

Figure 4B shows that the corresponding results for Y42F at the same pH of 7 are very different. The initial fluorescence change is now negative (dotted curve). This is not consistent with the presence of a wild-type I_2-like intermediate. In that case, the initial fluorescence change should be large and positive. The negative initial fluorescence change is however consistent with an intermediate with a protonated chromophore that has the chromophore κ^2 factor (orientation) of I_1 and the spectral overlap J of I_2. Such an intermediate will be tentatively called I_1H (protonated I_1). From Figure 4B, we note that $\Delta F/F$ becomes large and positive with two exponential rise times of 17 and 56 μs. The time, sign, and magnitude of this change are consistent with the transition from I_1H to I_2, since J would remain about the same whereas κ^2 decreases strongly. In the same time range, the ground-state relaxation from the intermediate spectral form (390 nm) to the yellow form (457 nm) may also contribute. In this transition, J decreases and κ^2 is presumably not altered significantly (no isomerization). Consequently, $\Delta F/F$ would also be positive for this transition. In view of the good common global fit (the fit curves are superimposed on the data) of the transient absorption and fluorescence signals, we interpret the positive phase in the transient fluorescence as a superposition of the P^{390} to P^{457} relaxation and the I_1H to I_2 transitions. The next negative change with time constant of 2.8 ms is similar to the wild-type transition at 2.4 ms and clearly due to the I_2 to I_2' transition. The final transition is the recovery with a time constant of 1.8 s. The main new insight from transient fluorescence is thus that the initial UV-absorbing intermediate with protonated chromophore does not have the chromophore orientation of a wild-type I_2 state but is consistent with an I_1-like orientation. This means that after isomerization and formation of the I_1 intermediate with deprotonated chromophore and two hydrogen bonds to E46 and T50, I_1 becomes protonated (presumably from E46) before the start of our data acquisition (< 50 ns), keeping the two hydrogen bonds and chromophore orientation. Figure 10 provides a scheme of the photocycle kinetics based on all of the kinetic data.

Kinetics of Proton Uptake/Release and Dye Binding. Transient absorption experiments were performed in the presence of the pH indicator dye BCP to learn about the kinetics of proton uptake and release as well as on transient dye binding. Measurements of the transient pH changes allow us to distinguish whether protonation changes are due to proton uptake from the aqueous bulk phase or due to intramolecular proton transfer. In wild type and a number of mutants, proton uptake is strictly coupled to the protonation of the chromophore in the formation of the I_2 intermediate (*23*). Transient dye binding, on the other hand, is coupled to the formation of the subsequent I_2' intermediate in which the protein partially unfolds, exposing a hydrophobic surface patch (*14*, *23*). The results of the transient pH indicator experiments are shown in Figure 5, at pH 7, close to the pK_a of the dye (6.3). Panels A and B of Figure 5 show the dye signal in the absence and presence of buffer, respectively, at four wavelengths near the absorption maximum of the deprotonated form of the dye (590 nm). Similar data were recorded at 9 wavelengths from 550 to 630 nm. The data of Figure 5B, in the presence of excess buffer, represent the kinetics of transient dye binding. They show that the dye absorption spectrum is transiently red-shifted with time constants of 230 μs and 1.9 ms. These time constants were obtained from a global fit of the time traces at the 9 wavelengths. The two amplitudes are about equal. In wild type, transient dye binding is associated with the formation of I_2' but occurs with a single time constant of about 2 ms (*23*). In the photocycle data for Y42F only a 1.25 ms component but no 230 μs component was detected. The dye binding data suggest however that the I_2 to I_2' transition in Y42F is biphasic. This may be difficult to detect by transient absorption measurements due to the great similarity of the spectra of the I_2 intermediates. The signal recovers in 1 s, which is the cycle recovery time.

Subtracting the data in the presence of buffer from those in its absence, we obtain the pure protonation signal shown in Figure 5C. There is no bulk proton concentration change until the uptake signal at 230 μs. Calibration of the signal leads to a proton uptake stoichiometry of 1.03. The 1.9 ms transition corresponding to the formation of I_2' is very weak as expected, and proton release occurs with the recovery of the cycle. There was no proton uptake at all in the 65 μs region that would correspond to formation of I_2.

The bulk protonation changes provide valuable information complementary to the photocycle data. Since the initial signal at 100 ns is zero, no external proton is taken up in the formation of

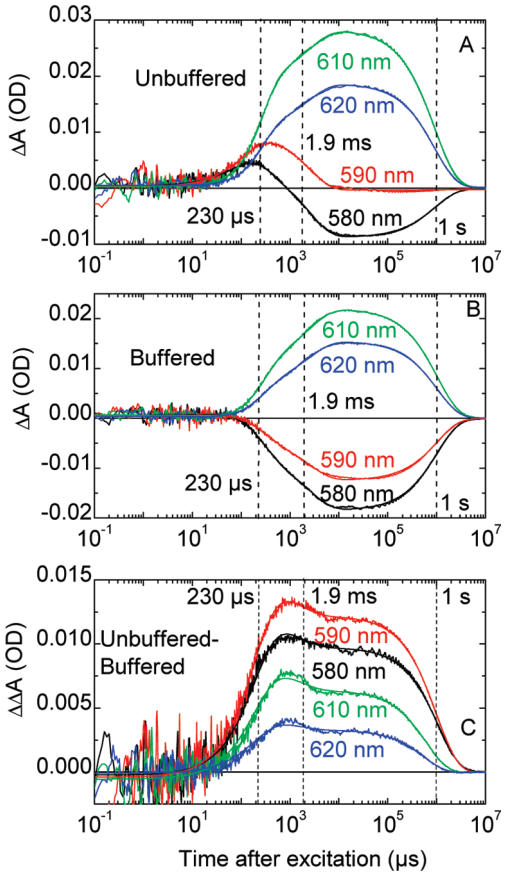

FIGURE 5: Transient absorbance changes after excitation at 470 nm of a Y42F solution in the presence of the pH indicator dye BCP. Measurements were performed at 9 wavelengths from 550 to 630 nm: (A) unbuffered; (B) buffered. For clarity, only the time traces at the four indicated wavelengths are plotted. (C) Protonation signal, acquired as the difference between the signals from (A) and (B). The dashed vertical lines represent the time constants of the global fit of the time traces at all 9 wavelengths in the time range of 5 μs to 10 s. Fit curves are indicated by the solid lines. Conditions for (A): pH 7.1, 20 °C, path length 5 mm, 20 mM KCl, 44 μM BCP, ground-state absorption of PYP (without dye) at 457 and 390 nm was 1 and 0.65 OD, respectively. Conditions for (B): 30 mM Tris was added as buffer.

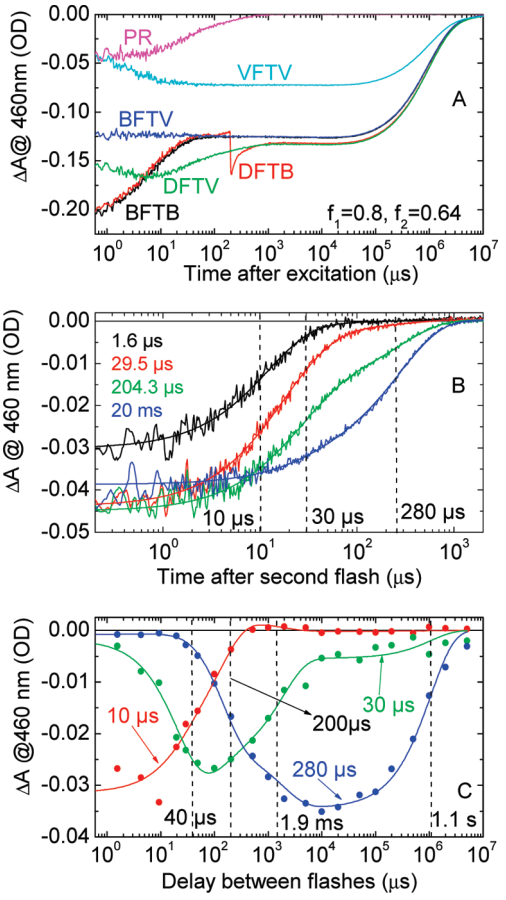

FIGURE 6: (A) Absorbance changes at 460 nm after single (460 or 355 nm) or double flash excitation (460 nm followed by 355 nm after a 200 μs delay). The double flash traces labeled DFTB and DFTV are triggered on the first flash (460 nm) and on the second flash (355 nm), respectively. Single flash signals with either blue (B, 460 nm) or violet (V, 355 nm) excitation and triggered on the first (BFTB) or second flash (BFTV, VFTV) are displayed as well. These are required to construct the photoreversal signal (PR) according to the method described in the text, with $f_1 = 0.8$ and $f_2 = 0.64$. (B) The photoreversal signals were measured at 460 nm at 21 delays ranging from 1.6 μs to 5.01 s, and the noise level was reduced using SVD as described in the text. For clarity, only the data at the indicated delays are shown. The solid lines represent a three-exponential global fit to all of the data with $\tau_1 = 10\,\mu$s, $\tau_2 = 30\,\mu$s, and $\tau_3 = 280\,\mu$s marked by the dashed vertical lines. (C) Dependence of the photoreversal amplitudes A_1, A_2, and A_3 on the delay. A_1 (red), A_2 (green), and A_3 (blue) are the amplitudes of the 10, 30, and 280 μs components, respectively, obtained from the global fit of the delay data of panel B. The dashed vertical lines at 40 μs, 200 μs, 1.9 ms, and 1.1 s indicate the values of the time constants for a global fit with four exponentials. The PR signals were measured with the same sample and under the same conditions as mentioned in Figure 2A.

the early UV-absorbing intermediate I_1H with protonated chromophore that is already present in the initial bleach (Figure 2B). Therefore, chromophore protonation in this intermediate must occur intramolecularly from an internal donor. Since three UV-absorbing intermediates, all with protonated chromophores, are present during the entire cycle, the proton that is taken up around 230 μs is not taken up by the chromophore but by some other proton acceptor group which may change its pK_a during the photocycle such as glutamate 46. Since no bulk proton concentration change is associated with the 5 μs relaxation time, we conclude that this transition between the yellow and intermediate spectral forms, which also involves a protonation change of the chromophore, must involve intramolecular proton transfer presumably via the hydrogen bond with Glu46. The presence of a strong dye binding signal suggests that a normal I_2' intermediate is formed in which a major conformational change has occurred. The proposed proton uptake and release steps are indicated in the scheme of Figure 10.

Photoreversal Kinetics with a Second Flash at 355 nm. As a consequence of the complexities of the photocycle with two dark species and three UV-absorbing intermediates, it was not possible to calculate the time courses of the intermediate populations for the Y42F mutant from the transient absorbance data and the intermediate spectra as we did for wild type (*13*, *24*). We therefore investigated the photoreversal kinetics, since this provides an alternative way to determine the time courses of the I_1H, I_2, and I_2' intermediates (*45*). In such experiments, the initial flash at 460 nm is followed after a defined time delay by a second flash at 355 nm which converts the UV-absorbing intermediates present at that time back to the dark state. The calculation of the photoreversal time traces from the double flash data is described in detail in ref *45*. Here, we will be very brief. The time traces at 460 nm are shown in Figure 6A. The trace labeled BFTB represents the response to a single blue flash at 460 nm, triggered

at that flash. DFTB is the double flash signal, i.e., the response to an initial blue flash followed after 200 μs by a violet flash at 355 nm, triggered on the first flash. The negative spike at 200 μs is due to the photoreversal. DFTV is the same signal, but now triggered on the second, violet flash. In this way the effect of the second, photoreversal flash is time-resolved. This signal has to be corrected for the fact that the second flash also excites molecules in the yellow and intermediate spectral forms that were not excited by the first flash. This effect is expressed by the time trace VFTV, the response to a single violet flash at 355 nm. This correction is larger in Y42F than in wild type, due to the presence of the intermediate spectral form which absorbs strongly in the UV. The VFTV trace clearly contains a component with a time constant of a few microseconds due to the relaxation between the two dark ground states (see also Figure 3A). To obtain the photoreversal signal (PR), the DFTV trace also has to be corrected for the contribution from those molecules that are not photoreversed by the second flash and continue along the cycle (BFTV). The weights of these two corrections, f_1 and f_2, were determined as described (*45*). The purple trace (PR) is the final photoreversal signal after these corrections. Similar experiments were carried out at 21 delays from 1.6 μs to 5 s. These data were subjected to SVD analysis. There are three significant singular value components, which correspond to the photoreversals from the three intermediates I_1H, I_2, and I_2' to the dark equilibrium (see below). The data were reconstructed using the first three singular values, leading to a reduction of the noise. Four of these traces for delays ranging from 1.6 μs to 20 ms are shown in Figure 6B. It is clear that the traces depend strongly on the delay and contain several time constants. A global fit of all 21 time traces to a sum of three exponentials led to a good fit with time constants $\tau_1 = 10\,\mu$s, $\tau_2 = 30\,\mu$s, and $\tau_3 = 280\,\mu$s. A fit with two exponentials was unsatisfactory. The dependencies of the corresponding amplitudes A_1, A_2, and A_3 on the delay are plotted in Figure 6C. For wild type, the photoreversal times of I_2 and I_2' are 60 and 380 μs (*45*). It is thus plausible that the reversal times of 30 and 280 μs are the corresponding times for the mutant Y42F. The 10 μs reversal time is then probably due to the I_1H intermediate. Since this time coincides with the relaxation time of the dark equilibrium, it is most likely an apparent time constant. After photoreversal from I_1H the dark equilibrium has to be reestablished. The actual photoreversal time from I_1H could thus be faster than 10 μs. With this assignment, the associated amplitudes A_1, A_2, and A_3 describe the time courses of the populations of the I_1H, I_2, and I_2' intermediates, respectively. The delay dependence of the three amplitudes shown in Figure 6C was fitted with a sum of four exponentials. The time constants of 40 μs, 200 μs, 1.9 ms, and 1.1 s are indicated by the dashed vertical lines. The times of 40 μs and 1.9 ms are in reasonable agreement with the photocycle times of 65 μs and 1.25 ms corresponding to the I_1H to I_2 and I_2 to I_2' transitions. The data show that I_1H decays to both I_2 and I_2'. The time courses of the I_2 and I_2' intermediates indicate that, as in wild type, these intermediates are in equilibrium and decay together. The 200 μs time is similar to the 230 μs observed in the proton uptake and dye binding kinetics. The time courses of I_2 and I_2' in Figure 6C support the idea derived from the dye binding experiments that their interconversion is biphasic. The photoreversal steps and the I_2/I_2' equilibrium are indicated in the scheme of Figure 10.

Combined Kinetics. The time constants obtained from the various kinetic methods differ somewhat. This is in part due to the fact that the experimental conditions, such as pH, salt concentration, buffer, and temperature, which affect the kinetics, were not exactly the same (different samples). The four methods have moreover different sensitivities for the same transition. Transient absorbance is for example very insensitive to the kinetics from I_2 and I_2' since these intermediates have very similar absorption spectra, whereas transient fluorescence has a large difference signal for this transition. In all, we detected five time constants. The 5−10 μs dark relaxation, the 50−100 μs transition between I_1H and I_2, the mysterious 230 μs proton uptake time, the 1−2 ms formation of I_2', and the recovery time of 1−2 s. We tested whether a joint global fit to selected time traces from all four methods was possible. For this purpose we selected eight time traces shown in Figure 7. The four time traces in Figure 7A are the transient absorbance at 460 nm (blue), the transient fluorescence (black), the dye binding (green), and the proton uptake (red). The four time traces in Figure 7B are the high signal-to-noise transient absorbance at 350 nm obtained using an LED and the delay time dependence of the three photoreversal components. Since the recovery time is most sensitive to the experimental conditions, this time constant was left open but kept in the 1−2 s range. This recovery time is of little interest for this study. A good joint fit of all eight traces was possible as shown by the curve fits in Figure 7. The four common time constants obtained, 8 μs, 50 μs, 230 μs, and 2 ms, are in the range obtained with the individual methods and are indicated by the dashed

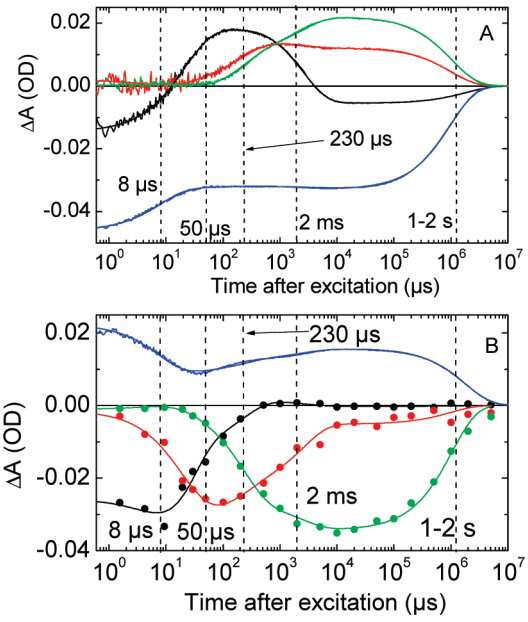

FIGURE 7: A global fit of eight representative photocycle time traces acquired with various experimental methods. These curves are picked from the previous figures. Some of the curves are scaled so that all signals are of comparable weight in the global fit. (A) Color code: black, transient fluorescence changes (from Figure 4B); red, proton signal measured at 590 nm (from Figure 5C); green, dye binding signal measured at 610 nm (from Figure 5B); blue, transient absorbance changes at 460 nm (from Figure 2A). (B) Black, red, and green filled circles: delay dependence of the photoreversal amplitudes of the 10, 30, and 280 μs photoreversal components, respectively (from Figure 6C). The blue curve represents the transient absorbance changes at 350 nm (from Figure 4B). The vertical dashed lines indicate the time constants for a global fit of all eight curves with a sum of five exponentials. The amplitudes and the time constants of the recovery transition were not fitted globally since these traces were measured under slightly different sample conditions, which mainly affect this transition. The solid lines are the fits.

vertical lines in Figure 7. These representative times are presented in the photocycle scheme of Figure 10.

Fourier Transform Infrared (FTIR) Spectroscopy. To measure the state of protonation of chromophore and Glu46, we used FTIR spectroscopy. FTIR light minus dark spectra were acquired using the apparatus shown in Supporting Information Figure S1 with background illumination at 475 nm. This setup allowed the simultaneous recording of the FTIR and UV−vis spectra of the sample. In this way, it was possible to monitor the intermediate/yellow dark equilibrium in the FTIR sample, to control the degree of bleaching by the background illumination, and to measure the UV−vis spectrum in the photostationary state. The latter was quite valuable to monitor the equilibrium between the two UV-absorbing intermediates I_2 and I_2'.

In Figure 8, the FTIR and UV−vis spectra of Y42F are compared with those of wild type at pH 7. Figure 8A shows the dark spectra, normalized at 280 nm (this is not quite exact since one out of five tyrosine residues is replaced by phenyalanine). The dotted and dashed lines are the spectral contributions of the intermediate and yellow spectral forms, respectively. These spectra were obtained by varying the KCl concentration from 0.5 to 4.5 M. A clean isosbestic point was obtained, suggesting a two-state equilibrium and allowing the calculation of the two spectra. We found that actually $\lambda_{max} \approx$ 387 nm for the intermediate spectral form, but we call this species P^{390} to conform with current nomenclature. The fractions of Y42F in the yellow and intermediate spectral forms are approximately 0.5 under these conditions. Figure 8B shows the UV−vis spectra of the FTIR samples under continuous illumination at 475 nm. The negative absorbance anomaly at 475 nm is an artifact due to the CW laser. The Y42F and wild-type samples are bleached to a similar extent (Figure 8C). The band with a maximum around 360 nm is due to the equilibrium between the I_2' and I_2 intermediates. It is clear from the light minus dark difference spectrum for Y42F shown in Figure 8C that both the yellow and intermediate spectral forms of Y42F are bleached, in accordance with the postulated rapid relaxation between the dark states. Excitation at 475 nm, a wavelength at which the intermediate spectral form does not absorb, depletes the yellow form, thereby perturbing the dark equilibrium. As more and more of the yellow form is bleached, the intermediate spectral form converts into the yellow form to reestablish the equilibrium.

The corresponding light minus dark FTIR difference spectra of wild type and Y42F are shown in Figure 8D. They are normalized by the same factor as the UV−vis spectra. The negative bands are due to the disappearing dark state, in the case of Y42F both the yellow and intermediate spectral forms. The positive bands arise from the mixture of photocycle intermediates in the photostationary state. From Figure 8B, we know that this consists mainly of I_2', the slowest intermediate of the cycle, that accumulates under steady-state illumination. The negative bands at 1058/1041 cm^{-1} and the positive bands at 1005 cm^{-1} are marker bands for the *trans* and *cis* forms of the chromophore, respectively (*49*). Clearly, chromophore isomerization occurs in Y42F to about the same extent as in wild type. This is consistent with the similar extent of bleach in the UV−vis spectra. Both forms of Y42F contribute. The bands at 1163, 1303, and 1480 cm^{-1} are marker bands for the deprotonated form of the chromophore (*49*, *50*). These marker bands are markedly reduced in intensity in Y42F with respect to wild type. We interpret this by postulating that the fraction of the dark state that is in the intermediate spectral form has a protonated chromophore and thus does not contribute to these bands. The reduction in intensity with respect to wild type is roughly in agreement with the fraction in the intermediate spectral form deduced from the UV−vis absorption spectrum. The bands at 1645 and 1624 cm^{-1} are due to the amide I band of the protein backbone and are evidence for the global structural change in the transition to the I_2' intermediate. The similarity in the amide I

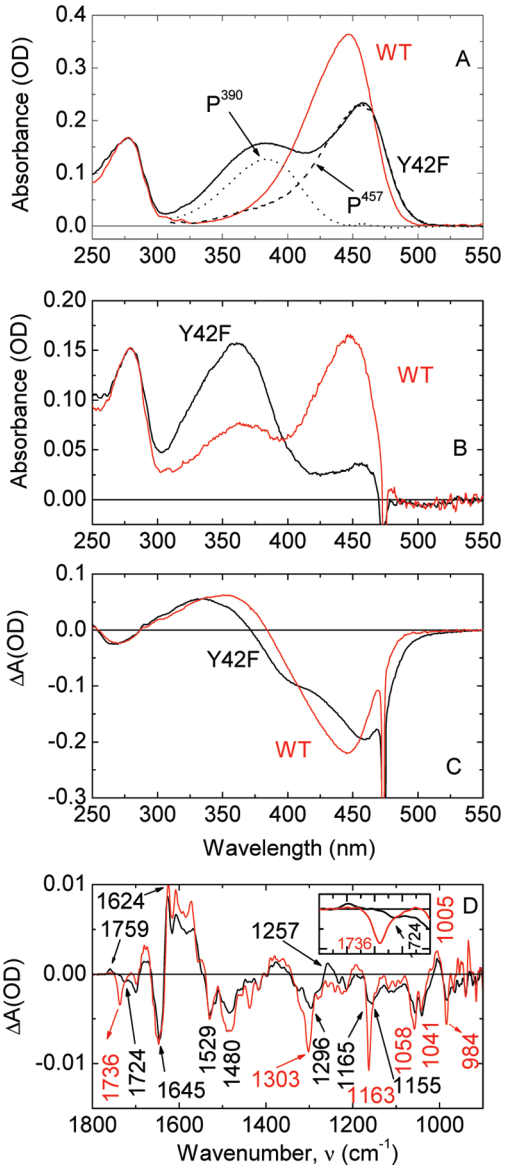

FIGURE 8: Comparison between UV−vis and FTIR spectra of WT and Y42F at pH 7 in the dark and with background illumination. Each set of spectra was measured with the same sample. (A) UV−vis dark absorption spectra. The spectra of the yellow and intermediate spectral forms are indicated by the dashed and dotted lines, respectively. (B) UV−vis absorption spectra under continuous background illumination at 475 nm. (C) Light minus dark UV−vis absorption spectra. (D) FTIR light minus dark difference spectra: red curves, WT; black curves, Y42F. The UV−vis spectra were normalized at ~280 nm. The same scaling factor was used for the scaling of the FTIR spectra. The wavenumber range 1700−1780 cm^{-1} is enlarged in the inset. The wavenumbers of the major peaks are indicated for both proteins. Conditions: WT, 20 °C, 6 μm path length, pH 7, 100 mM KCl, 10 mM Tris (1 μL of 500 mM KCl was placed at the center of one of the plates and 1 μL of 50 mM Tris and 3 μL of WT each at pH 7 were added); Y42F, 20 °C, 6 μm path length, pH 7, no additional KCl, 10 mM Tris (1 μL of 50 mM Tris at pH 7 is placed at the center of one of the plates; 4 μL of Y42F is then added to the Tris).

and II region shows that, in Y42F, a wild-type-like I_2' intermediate is formed.

Of greatest interest are the negative bands at 1736 cm^{-1} (wild type) and 1724 cm^{-1} (Y42F). These bands are due to the carbonyl stretch vibration of the protonated carboxyl group of E46 (*19*, *20*). In D_2O, the 1724 cm^{-1} band shifts to 1714 cm^{-1} (data not shown). This spectral region is shown enlarged in the inset of Figure 8D. The lowering of this frequency in Y42F means that the hydrogen bond between E46 and the deprotonated chromophore is stronger in the yellow form of Y42F than in wild type. Its lower intensity in the mutant may be interpreted as follows. In the yellow form, E46 is protonated and the chromophore deprotonated. Our working hypothesis is that in the intermediate spectral form E46 is deprotonated and the chromophore protonated. The latter is supported by resonance Raman measurements of the intermediate spectral form (*39*). The fraction of Y42F in the intermediate spectral form will thus not contribute to the intensity of the 1724 cm^{-1} band, leading to its lower intensity compared to wild type. The positive band at 1759 cm^{-1} is most likely also due to E46. It suggests that, in the I_2' intermediate of Y42F, E46 is protonated. The frequency value of 1759 cm^{-1} is consistent with a protonated E46 without a hydrogen bond (*51*). The fact that the intensities of the marker bands for the deprotonated chromophore (1163, 1480, 1303 cm^{-1}) and the marker band for the protonated E46 are both markedly reduced to approximately the same extent compared to wild type argues strongly in favor of a protonated chromophore and a deprotonated E46 in the intermediate spectral form. The intensities may be normalized at the 1058/1041 cm^{-1} *trans* marker bands, since the chromophores of both the yellow and intermediate spectral forms isomerize upon excitation by the 475 nm background light. The FT Raman spectrum of Y42F already showed that the ratio of the intensities at 1163 cm^{-1} (deprotonated chromophore) and 1058/1041 cm^{-1} (*trans* chromophore, which measures the extent of isomerization) was smaller in Y42F than in wild type (*36*).

These results about the protonation states of E46 and the chromophore are supported by experiments in which the equilibrium was gradually shifted. This can be accomplished by changing the concentrations of chaotropes or kosmotropes or by temperature change (*36*, *38*). Experiments with the chaotrope KCl and the kosmotrope $(NH_4)_2SO_4$ which shift the equilibrium in the direction of the intermediate spectral form and the yellow form, respectively showed that the frequency of the 1724 cm^{-1} band was unaffected (data not shown). The strength of the hydrogen bond thus does not depend on the position of the equilibrium. Raising the temperature shifts the equilibrium in the direction of the intermediate spectral form (*38*). From the observation of an isosbestic point, it was concluded that this is a two-state equilibrium up to 40 °C (*38*). The apparent wavelength maximum of the intermediate spectral form shifts to lower wavelengths as the temperature is raised, since the amplitude of the yellow form decreases. Beyond 40 °C a third species absorbing around 350 nm appears, and the isosbestic point is lost (*38*). A combined UV−vis/FTIR experiment was performed for temperatures ranging from 2 to 41.4 °C. Figure 9A shows how the equilibrium shifts toward the intermediate form with increasing temperature. Figure 9B shows that the sample was almost completely bleached by the 475 nm background illumination. The light minus dark FTIR spectra of Figure 9C indicate that the intensities of the 1480 and 1165 cm^{-1} marker bands for the deprotonated chromophore decrease significantly with increasing temperature, i.e., with increasing amount of the intermediate

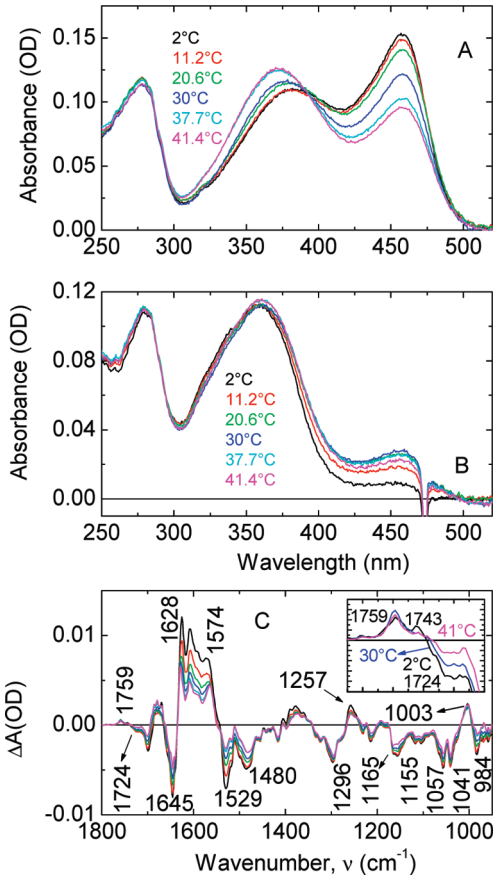

FIGURE 9: Temperature dependence of optical and FTIR spectra of Y42F. (A) Dark and (B) light (475 nm background illumination) optical spectra and (C) light minus dark FTIR spectra. Color code for temperatures: black, 2 °C; red, 11.2 °C; green, 20.6 °C; blue, 30 °C; light blue, 37.7 °C; pink, 41.4 °C. The wavenumber range 1700−1780 cm^{-1} is enlarged in the inset of panel C. Conditions: 6 μm path length, pH 7, no additional KCl, 65 mM Tris (3 μL of Y42F stock solution (suspended in 64 mM Tris at pH 7) was placed in the center of the one of the plates, 1 μL of 200 mM Tris at pH 7 was added, and the plates were closed immediately).

spectral form. The inset shows the temperature dependence in the 1700−1800 cm^{-1} range. The frequency of the 1724 cm^{-1} band position is unaffected but its intensity decreases with increasing temperature. The concomitant decrease of the 1724 and 1165/1480 cm^{-1} marker bands when the equilibrium is shifted toward the intermediate spectral form and less of the yellow form remains is a further argument that, in the intermediate spectral form, E46 is deprotonated and the chromophore protonated. The protonation states of E46 and the chromophore derived from FTIR are indicated in the photocycle scheme of Figure 10.

DISCUSSION

We characterized the mutant Y42F with the goal of understanding the nature of the intermediate spectral form and the role of the hydrogen bonds of the chromophore with Y42 and E46. In the yellow form of this mutant, the very short hydrogen bond between the chromophore and Y42 observed in wild type is replaced by a longer and weaker one with T50 (*36*). This strengthens the adjacent hydrogen bond with E46, which was already unusually strong in wild type and which becomes shorter by 0.07 Å (*36*). These two hydrogen bonds share the oxyanion of the chromophore as the common acceptor. The proton affinity of the chromophore in the second hydrogen bond, with E46, is thus

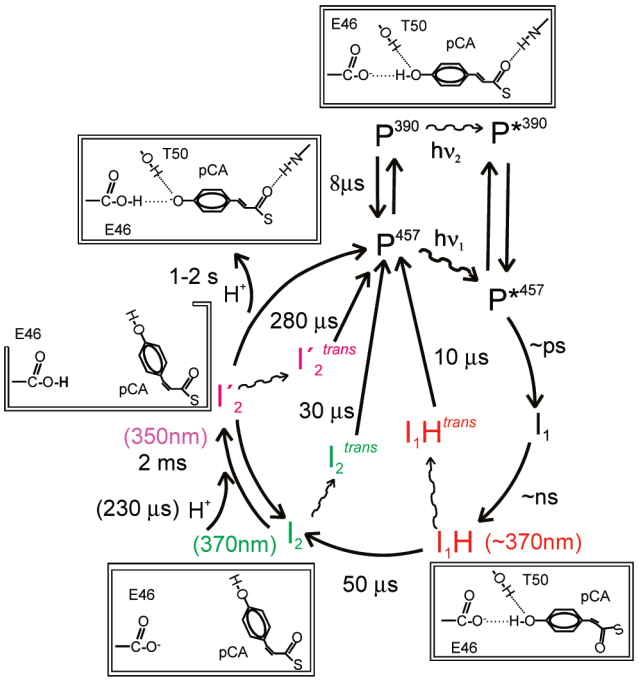

FIGURE 10: Proposed model for the photocycle of PYP mutant Y42F at neutral pH. The yellow (P^{457}) and intermediate forms (P^{390}) are in equilibrium in the dark, interconverting with a time constant of 8 μs. It is proposed that the two forms share a common photocycle by excited state proton transfer. After photoisomerization and formation of I_1, the I_1H intermediate is formed within 100 ns, which in turn decays to I_2 in 50 μs. The I_2/I_2' equilibrium is formed with a time constant of 2 ms. A proton is taken up from the solvent with a time constant of 230 μs. Finally, the dark equilibrium recovers from the I_2/I_2' equilibrium during the 1−2 s transition with the release of a proton. These time constants are taken from the joint fit of the representative data of Figure 7. The values of the absorbance maxima are indicated in parentheses. For each intermediate, the proposed hydrogen bonding and protonation states of the chromophore and E46 are indicated. The photoreversal time constants of the I_1H, I_2, and I_2' intermediates are 10, 30, and 280 μs, respectively. The chromophore configuration of these intermediates changes from *cis* to *trans* immediately after the second flash.

increased in Y42F. The coupling between the two hydrogen bonds is caused by the electrostatic interaction between the charge distributions in these bifurcated hydrogen bonds which are linked via the common acceptor. In wild type the hydrogen bond with E46 is very short. Neutron diffraction experiments in wild type showed that the proton in this hydrogen bond is approximately in the middle between donor and acceptor and is shared by the two oxygens (*27*). It is one of the best documented examples of a low-barrier hydrogen bond (LBHB) in proteins (*27*). The presence of the E46 carboxylic acid group and presumably this hydrogen bond are essential for the occurrence of the intermediate spectral form (*38*).

Our observation of a decrease in the frequency of the carbonyl stretching frequency of the protonated carboxyl group of E46 from 1736 cm^{-1} in wild type to 1724 cm^{-1} in the yellow form of Y42F is direct evidence that the E46−chromophore hydrogen bond is stronger in this mutant. When the oxygens of the donor and acceptor move closer together, the barrier for proton transfer is lowered and the probability of proton transfer increased. We therefore believe that the key to understanding the intermediate spectral form and its properties is the protonation equilibrium between the carboxylic acid group of E46 and *p*-hydroxycinnamoyl chromophore indicated in the scheme of Figure 10. Resonance Raman experiments suggested that the chromophore is protonated in the intermediate form (*39*) but provided no information on the protonation state of E46. Our FTIR results not only support a protonated chromophore but also provide strong evidence for a deprotonated E46 in the intermediate spectral form. These conclusions were derived from a comparison of the relative intensities of the marker bands for E46 protonation and chromophore deprotonation in wild type and Y42F as well as from the changes in these intensities when the equilibrium is shifted toward the intermediate spectral form.

The protons in the two bifurcated hydrogen bonds repel each other. Replacing the strong hydrogen bond with Y42 by the weaker one with T50 would lead to reduced Coulomb repulsion, allowing the proton in the neighboring hydrogen bond with E46 to move closer to the chromophore oxygen. The mutation alters the interaction between the two hydrogen bonds, strengthening the hydrogen bond with E46, lowering the barrier for proton transfer in that hydrogen bond, facilitating proton transfer, and shifting the protonation equilibrium to the side of the chromophore.

In recent ^{1}H NMR experiments, the chemical shifts of the protons in the two hydrogen bonds of the chromophore with E46 and Y42 were assigned (*30*). From observations of the effect of replacing H by D on the chemical shifts it was concluded that these two hydrogen bonds interact in an anticooperative way: if one gets stronger, the other gets weaker. The conclusion of coupling between the two hydrogen bonds from NMR is in agreement with the interpretation of our observations. Moreover, in the Y42F mutant, the chemical shift assigned to the proton in the hydrogen bond to E46 was even further downfield than in wild type (*30*), suggesting migration of the proton in the E46−chromophore hydrogen bond toward the chromophore oxygen, in agreement with our FTIR result on the frequency shift of the E46 carbonyl vibration.

From our photocycle measurements we concluded that the protonation equilibrium between the two dark states of Y42F relaxes rapidly with a time constant of about 5 μs. This relaxation time is independent of whether the yellow or intermediate spectral form is depleted, and its amplitude spectrum agrees with the difference spectrum between the yellow and intermediate spectral forms. These observations provide strong evidence for our interpretation of the 5 μs transition. Since the equilibrium is temperature dependent, a temperature jump experiment with nanosecond perturbation of the equilibrium, e.g., by IR heating of the water, and detection of the transient absorption would provide direct proof for our contention. However, there is no need for this, since a number of additional experiments support our hypothesis. In the presence of the kosmotrope $(NH_4)_2SO_4$, which shifts the equilibrium almost completely to the yellow form, the microsecond component was absent (data not shown). Excitation at 475 nm, where the intermediate form does not significantly absorb, leads to bleaching of the intermediate spectral form, as a consequence of the rapid dark state equilibrium (Figure 8C). We note that similar relaxation kinetics between two dark spectral forms absorbing in the UV and around 450 nm was observed previously with the mutants E46Q and E46A at pH values close to the pK_a for chromophore protonation in the dark (*33*).

For the relaxation time of the dark equilibrium between the two forms we obtained a value of 5 μs. The corresponding rate is the sum of the rate constants for the forward and backward reactions. Is this value reasonable for proton transfer via a

hydrogen bond in a low dielectric protein matrix? Another question is whether the assumed model of proton transfer in a double-well potential is oversimplified. The second minimum with the proton near the chromophore oxygen may only be generated by some structural change in the chromophore environment. In the double mutant Y42F/T50V, the chromophore has only one hydrogen bond with Glu46, and the equilibrium at neutral pH is almost entirely on the side of the intermediate spectral form (*38*). The transient breaking of the T50−chromophore hydrogen bond may thus provide a mechanism for proton transfer from Glu46 to the chromophore and formation of the intermediate spectral form. This idea is supported by quantum chemical calculations which show that the pK_a of the chromophore increases by removal of the hydrogen bond between the chromophore and Y42 (*39*). Breaking of the hydrogen bond with T50 will likewise stabilize the protonated chromophore. We do not know whether the hydrogen bond with T50 is absent in the intermediate spectral form since its structure has not been determined.

Both forms are photoactive and have virtually identical photocycles apart from the signs of the relaxation components. The latter have amplitudes of opposite sign in accordance with the equilibrium model. The virtual identity of the two photocycles suggests that they are strongly coupled. One plausible mechanism for this coupling is excited state proton transfer (ESPT). Exciting the P^{390} intermediate spectral form leads to deprotonation of the chromophore in the excited state and proton transfer presumably to the acceptor E46. Thereafter, the cycle is the same as for the P^{457} yellow form which has a deprotonated chromophore to begin with. The photocycle scheme of Figure 10 depicts the dark equilibrium and the coupling of the two cycles. Such a mechanism is also consistent with the fluorescence excitation spectrum of Y42F (*36*). The chromophore emission originates from the excited state of P^{457}, but the excitation spectrum is proportional to the absorption spectrum and includes the contribution from P^{390} as a shoulder (*36*).

The green fluorescent protein (GFP) is the best known example for the operation of such a mechanism (*52*, *53*). The analogies between the Y42F mutant of PYP and the green fluorescent protein are remarkable. The *p*-hydroxybenzylideneimidazolinone chromophore of GFP is formed through the cyclization and oxidation of the three amino acids Ser65-Tyr66-Gly67. In wild-type GFP, the chromophore is in an equilibrium between a neutral form A absorbing at 395 nm in which the chromophore hydroxyl group is protonated and an anionic form B absorbing at 475 nm in which the hydroxyl group is deprotonated. The A and B species correspond to the intermediate spectral and yellow forms of the *p*-hydroxycinnamoyl chromophore of Y42F, respectively. In both proteins, the hydroxyl group is part of a hydrogen-bonded network inside the protein, and the fluorescence originates from the species with deprotonated chromophore. It was shown for GFP that excitation of the A form leads in several picoseconds to formation of an anionic species in the excited state by deprotonation of the chromophore and concomitant protonation of the carboxylate group of E222 (*53*). We suggested, from the observation that the photocycles of the yellow and intermediate spectral forms of Y42F are virtually identical, that ESPT occurs from the protonated chromophore to E46 upon excitation of the intermediate spectral form. ESPT also provides a straightforward explanation for the observed excitation spectrum of the Y42F chromophore fluorescence (*36*).

The common photocycle, here investigated from 50 ns to seconds, does not have a red-shifted I_1 intermediate in this time range as is the case for wild type. From picosecond spectroscopy, it is known, however (*40*), that an early I_1 intermediate is formed in 30 ps, i.e., much faster than in wild type (30 ns). The first intermediate we can observe absorbs in the UV and already has a protonated chromophore. We called this intermediate I_1H since it has a chromophore structure (orientation) like I_1 but an absorption spectrum like I_2: hence protonated I_1. To reach this conclusion, we used transient fluorescence which is sensitive to both the spectrum and chromophore orientation of an intermediate (*25*).

An early blue-shifted intermediate called PYP-BL was observed in wild type by low-temperature spectroscopy (*55*). We believe that PYP-BL is unrelated to I_1H for the following reasons. PYP-BL occurs between I_0 and I_1, whereas I_1H follows I_1. I_1H has its wavelength maximum at about 370 nm, whereas PYP-BL absorbs maximally at about 400 nm. PYP-BL occurs exclusively at low temperature as a trapped state in a branched photocycle and was never observed in time-resolved experiments at room temperature, whereas I_1H is observed at room temperature in an unbranched cycle.

I_1H decays to an I_2-like intermediate in about 50 μs. The presumed signaling state I_2' is formed in a biphasic manner with time constants of 230 μs and 2 ms. From photoreversal kinetics, the time courses of I_2 and I_2' were determined, showing that these intermediates are in equilibrium from 1 ms onward as in wild type. Dye binding and FTIR experiments indicate that the I_2' state in Y42F is similar to that in wild type with a major conformational change.

Proton uptake, as measured with the pH indicator dye bromocresol purple (BCP), occurs with a rise time of 230 μs. From the absence of additional proton uptake processes, two conclusions can be drawn. First, the chromophore protonation change during the 5 μs yellow/intermediate relaxation is an intramolecular process, in agreement with our hypothesis that this rapid proton transfer occurs via the hydrogen bond with E46. Second, since the proton uptake signal is zero at the beginning of data acquisition, when the I_1H intermediate with protonated chromophore has already formed, we can conclude that the protonation of the chromophore occurring in the formation of I_1H is also an intramolecular event. The most likely candidate for the proton donor is E46. We note that the response time of the dye is in the range of a few microseconds (*23*). Earlier bulk protonation changes would then be detected with a delay. No such signals were observed, however. The proton taken up with the 230 μs time constant cannot be accepted by the chromophore since both I_2 and I_2' have protonated chromophores. One potential acceptor candidate is E46, since the FTIR signal shows a positive band at 1759 cm^{-1}. In time-resolved FTIR experiments with wild-type PYP a similar positive band was observed at 1759 cm^{-1} at 450 μs after the flash, which was assigned to the protonated form of E46 (*19*). In light minus dark FTIR difference spectra with background illumination a similar positive band was observed at 1747 cm^{-1} for wild type at pH 5 (*56*). So the band we observe in Y42F is also probably due to E46. The high wavenumber is consistent with a protonated E46 without a hydrogen bond (*51*). In our proposed photocycle scheme of Figure 10 E46 deprotonates in the formation of I_1H and becomes protonated in the global conformational change associated with the formation of I_2'. Our value of 1 for the proton uptake stoichiometry in the formation of I_2' is in agreement with the proposed simultaneous protonation change of E46.

The major difference between the Y42F and wild-type photocycles is the early formation of a protonated I_1H intermediate. Instead of two, there are three UV-absorbing intermediates with protonated chromophores in this mutant. The first of these, I_1H, is a new intermediate. The proposed scheme of the Y42F photocycle is shown in Figure 10.

SUMMARY

We showed by FTIR that the hydrogen bond between Glu46 and the oxygen of the chromophore is stronger in the yellow form of Y42F than in wild type. This strengthening is attributed to the replacement of the adjacent Y42−chromophore hydrogen bond of wild type by a weaker hydrogen bond with T50 in the Y42F mutant. In the shorter Glu46−chromophore hydrogen bond of the yellow form of Y42F, the barrier for proton transfer is lowered, allowing the bridging proton to cross the barrier forming the intermediate spectral form. Our FTIR data indicate that the chromophore is protonated and Glu46 deprotonated in the intermediate spectral form. By selective flash excitation of either of the two forms, this dark protonation equilibrium is perturbed and returns to equilibrium with a relaxation time of 5 μs. Excitation of the yellow or intermediate spectral form at 460 or 355 nm, respectively, leads to the same photocycle in the 50 ns to 10 s time range, indicating that the two cycles are strongly coupled, probably by excited state proton transfer. The common photocycle differs from that of wild type in two significant ways. No I_1-like intermediate with deprotonated chromophore is observed in our time range from 50 ns to seconds. Instead, using transient fluorescence spectroscopy an additional early intermediate with protonated chromophore was observed (I_1H) probably with an I_1-like chromophore configuration.

ACKNOWLEDGMENT

We thank Dr. Peter Tolstoy and Dr. Berthold Borucki for helpful comments and discussions.

SUPPORTING INFORMATION AVAILABLE

The layout of the combined FTIR/UV−vis fiber-optic spectrometer (Figure S1). This material is available free of charge via the Internet at http://pubs.acs.org.

REFERENCES

1. Cusanovich, M. A., and Meyer, T. E. (2003) Photoactive yellow protein: A prototypic PAS domain sensory protein and development of a common signaling mechanism. *Biochemistry 42*, 4759–4770.
2. Hellingwerf, K. J., Hendriks, J., and Gensch, T. (2003) Photoactive yellow protein, a new type of photoreceptor protein: Will this "yellow lab" bring us where we want to go? *J. Phys. Chem. A 107*, 1082–1094.
3. Imamoto, Y., and Kataoka, M. (2007) Structure and photoreaction of photoactive yellow protein, a structural prototype of the PAS domain superfamily. *Photochem. Photobiol. 83*, 40–49.
4. Kumauchi, M., Hara, M. T., Stalcup, P., Xie, A., and Hoff, W. D. (2008) Identification of six new photoactive yellow proteins-diversity and structure-function relationships in a bacterial blue light photoreceptor. *Photochem. Photobiol. 84*, 956–969.
5. Taylor, B. L., and Zhulin, I. B. (1999) PAS domains: Internal sensors of oxygen, redox potential, and light. *Microbiol. Mol. Biol. Rev. 63*, 479–506.
6. Pellequer, J. L., Wager-Smith, K. A., Kay, S. A., and Getzoff, E. D. (1998) Photoactive yellow protein: A structural prototype for the three-dimensional fold of the PAS domain superfamily. *Proc. Natl. Acad. Sci. U.S.A. 95*, 5884–5890.
7. Borgstahl, G. E. O., Williams, D. R., and Getzoff, E. D. (1995) 1.4 Å Structure of photoactive yellow protein, a cytosolic photoreceptor: Unusual fold, active site and chromophore. *Biochemistry 34*, 6278–6287.
8. Ihee, H., Rajagopal, S., Srajer, V., Pahl, R., Anderson, S., Schmidt, M., Schotte, F., Anfinrud, P. A., Wulff, M., and Moffat, K. (2005) Visualizing reaction pathways in the photoactive yellow protein from nanoseconds to seconds. *Proc. Natl. Acad. Sci. U.S.A. 102*, 7145–7150.
9. Düx, P., Rubinstenn, G., Vuister, G. W., Boelens, R., Mulder, F. A. A., Hard, K., Hoff, W. D., Kroon, A. R., Crielaard, W., Hellingwerf, K. J., and Kaptein, R. (1998) Solution structure and backbone dynamics of the photoactive yellow protein. *Biochemistry 37*, 12689–12699.
10. Groot, M. L., van Wilderen, L. J. G. W., Larsen, D. S., van der Horst, M. A., van Stokkum, I. H. M., Hellingwerf, K. J., and van Grondelle, R. (2003) Initial steps of signal generation in photoactive yellow protein revealed with femtosecond mid-infrared spectroscopy. *Biochemistry 42*, 10054–10059.
11. Heyne, K., Mohammed, O. F., Usman, A., Dreyer, J., Nibbering, E. T. J., and Cusanovich, M. A. (2005) Structural evolution of the chromophore in the primary stages of *trans*/*cis* isomerization in photoactive yellow protein. *J. Am. Chem. Soc. 127*, 18100–18106.
12. Hoff, W. D., van Stokkum, I. H. M., van Ramesdonk, H.-J., van Brederode, M. E., Brouwer, A. M., Fitch, J. C., Meyer, T. E., van Grondelle, R., and Hellingwerf, K. J. (1994) Measurement and global analysis of the absorbance changes in the photocycle of the photoactive yellow protein from *Ectothiorhodospira halophila*. *Biophys. J. 67*, 1691–1705.
13. Borucki, B., Joshi, C. P., Otto, H., Cusanovich, M. A., and Heyn, M. P. (2006) The transient accumulation of the signaling state of photoactive yellow protein is controlled by the external pH. *Biophys. J. 91*, 2991–3001.
14. Meyer, T. E., Tollin, G., Hazzard, J. H., and Cusanovich, M. A. (1989) Photoactive yellow protein from the purple phototrophic bacterium *Ectothiorhodospira halophila*. Quantum yield of photobleaching and effects of alcohols, glycerol and sucrose on kinetics of photobleaching and recovery. *Biophys. J. 56*, 559–564.
15. Rubinstenn, G., Vuister, G. W., Mulder, F. A. A., Düx, P. E., Boelens, R., Hellingwerf, K. J., and Kaptein, R (1998) Structural and dynamic changes of photoactive yellow protein during its photocycle in solution. *Nat. Struct. Biol. 5*, 568–570.
16. Chen, E. F., Gensch, T., Gross, A. B., Hendriks, J., Hellingwerf, K. J., and Kliger, D. S. (2003) Dynamics of protein and chromophore structural changes in the photocycle of photoactive yellow protein monitored by time-resolved optical rotatory dispersion. *Biochemistry 42*, 2062–2071.
17. Harigai, M., Imamoto, Y., Kamikubo, H., Yamazaki, Y., and Kataoka, M. (2003) Role of an N-terminal loop in the secondary structural change of photoactive yellow protein. *Biochemistry 42*, 13893–13900.
18. Imamoto, Y., Kamikubo, H., Harigai, M., Shimizu, N., and Kataoka, M. (2002) Light-induced global conformational change of photoactive yellow protein in solution. *Biochemistry 41*, 13595–13601.
19. Brudler, R., Rammelsberg, R., Woo, T. T., Getzoff, E. D., and Gerwert, K. (2001) Structure of the I_1 early intermediate of photoactive yellow protein by FTIR spectroscopy. *Nat. Struct. Biol. 8*, 265–270.
20. Xie, A., Kelemen, L., Hendriks, J., White, B. J., Hellingwerf, K. J., and Hoff, W. D. (2001) Formation of a new buried charge drives a large-amplitude protein quake in photoreceptor activation. *Biochemistry 40*, 1510–1517.
21. Hoersch, D., Otto, H., Joshi, C. P., Borucki, B., Cusanovich, M. A., and Heyn, M. P. (2007) Role of a conserved salt bridge between the PAS core and the N-terminal domain in the activation of the photoreceptor photoactive yellow protein. *Biophys. J. 93*, 1687–1699.
22. Van Brederode, M., Hoff, W. D., Van Stokkum, I. H. M., Groot, M.-L., and Hellingwerf, K. J. (1996) Protein folding dynamics applied to the photocycle of the photoactive yellow protein. *Biophys. J. 71*, 365–380.
23. Borucki, B., Devanathan, S., Otto, H., Cusanovich, M. A., Tollin, G., and Heyn, M. P. (2002) Kinetics of proton uptake and dye binding by photoactive yellow protein in wild type and in the E46Q and E46A mutants. *Biochemistry 41*, 10026–10037.
24. Joshi, C. P., Borucki, B., Otto, H., Meyer, T. E., Cusanovich, M. A., and Heyn, M. P. (2006) Photocycle and photoreversal of photoactive yellow protein at alkaline pH: Kinetics, intermediates and equilibria. *Biochemistry 45*, 7057–7068.
25. Hoersch, D., Otto, H., Cusanovich, M. A., and Heyn, M. P. (2008) Distinguishing chromophore structures of photocycle intermediates of the photoreceptor PYP by transient fluorescence and energy transfer. *J. Phys. Chem. B 112*, 9118–9125.

26. Lee, B. C., Croonquist, P. A., Sosnick, T. R., and Hoff, W. D. (2001) PAS domain receptor photoactive yellow protein is converted to a molten globule state upon activation. *J. Biol. Chem. 276*, 20821–20823.
27. Yamaguchi, S., Kamikubo, H., Kurihara, K., Kuroki, R., Niimura, N., Shimizu, N., Yamazaki, Y., and Kataoka, M. (2009) Low-barrier hydrogen bond in photoactive yellow protein. *Proc. Natl. Acad. Sci. U.S.A. 106*, 440–444.
28. Anderson, S., Crosson, S., and Moffat, K. (2004) Short hydrogen bonds in photoactive yellow protein. *Acta Crystallogr. 60*, 1008–1016.
29. Fisher, S. Z., Anderson, S., Henning, R., Moffat, K., Langan, P., Thiyagarajan, P., and Schultz, A. J. (2007) Neutron and X-ray structural studies of short hydrogen bonds in photoactive yellow protein (PYP). *Acta Crystallogr. D 63*, 1178–1184.
30. Sigala, P. A., Tsuchida, M. A., and Herschlag, D. (2009) Hydrogen bond dynamics in the active site of photoactive yellow protein. *Proc. Natl. Acad. Sci. U.S.A. 106*, 9232–9237.
31. Xie, A., Hoff, W. D., Kroon, A. R., and Hellingwerf, K. J. (1996) Glu46 donates a proton to the 4-hydroxycinnamate anion chromophore during the photocycle of photoactive yellow protein. *Biochemistry 35*, 14671–14678.
32. Devanathan, S., Brudler, R., Hessling, B., Woo, T. T., Gerwert, K., Getzoff, E. D., Cusanovich, M. A., and Tollin, G. (1999) Dual photoactive species in Glu46Asp and Glu46Ala mutants of photoactive yellow protein: A pH-driven color transition. *Biochemistry 38*, 13766–13772.
33. Borucki, B., Otto, H., Joshi, C. P., Gasperi, C., Cusanovich, M. A., Devanathan, S., Tollin, G., and Heyn, M. P. (2003) pH dependence of the photocycle kinetics of the E46Q mutant of photoactive yellow protein: Protonation equilibrium between I_1 and I_2 intermediates, chromophore deprotonation by hydroxyl uptake, and protonation relaxation of the dark state. *Biochemistry 42*, 8780–8790.
34. Philip, A. F., Eisenman, K. T., Papadantonakis, G. A., and Hoff, W. D. (2008) Functional tuning of photoactive yellow protein by active site residue 46. *Biochemistry 47*, 13800–13810.
35. Mihara, K., Hisatomi, O., Imamoto, Y., Kataoka, M., and Tokunaga, F. (1997) Functional expression and site-directed mutagenesis of photoactive yellow protein. *J. Biochem. 121*, 876–880.
36. Brudler, R., Meyer, T. E., Genick, U. K., Devanathan, S., Woo, T. T., Millar, D. P., Gerwert, K., Cusanovich, M. A., Tollin, G., and Getzoff, E. D. (2000) Coupling of hydrogen bonding to chromophore conformation and function in photoactive yellow protein. *Biochemistry 39*, 13478–13486.
37. Imamoto, Y., Koshimizu, H., Mihara, K., Hisatomi, O., Mizukami, T., Tsujimoto, K., Kataoka, M., and Tokunaga, F. (2001) Roles of amino acid residues near the chromophore of photoactive yellow protein. *Biochemistry 40*, 4679–4685.
38. Meyer, T. E., Devanathan, S., Woo, T., Getzoff, E. D., Tollin, G., and Cusanovich, M. A. (2003) Site-specific mutations provide new insights into the origin of pH effects and alternative spectral forms in the photoactive yellow protein from *Halorhodospira halophila*. *Biochemistry 42*, 3319–3325.
39. El-Mashtoly, S. F., Unno, M., Kumauchi, M., Hamada, N., Fujiwara, K., Sasaki, J., Imamoto, Y., Kataoka, M., Tokunaga, F., and Yamauchi, S. (2004) Resonance Raman spectroscopy reveals the origin of an intermediate wavelength form in photoactive yellow protein. *Biochemistry 43*, 2279–2287.
40. Devanathan, S., Lin, S., Cusanovich, M. A., Woodbury, N., and Tollin, G. (2001) Early photocycle kinetic behavior of the E46A and Y42F mutants of photoactive yellow protein: Femtosecond spectroscopy. *Biophys. J. 81*, 2314–2319.
41. Kyndt, J. A., Vanrobaeys, F., Fitch, J. C., Devreese, B. V., Meyer, T. E., Cusanovich, M. A., and Van Beeumen, J. J. (2003) Heterologous production of *Halorhodospira halophila* holo-photoactive yellow protein through tandem expression of the postulated biosynthetic genes. *Biochemistry 42*, 965–970.
42. Kyndt, J. A., Hurley, J. K., Devreese, B., Meyer, T. E., Cusanovich, M. A., Tollin, G., and Van Beeumen, J. J. (2004) *Rhodobacter capsulatus* photoactive yellow protein: Genetic context, spectral and kinetics characterization, and mutagenesis. *Biochemistry 43*, 1809–1820.
43. Borucki, B., Otto, H., and Heyn, M. P. (1999) Reorientation of the retinylidene chromophore in the K, L and M intermediates of bacteriorhodopsin from time-resolved linear dichroism: Resolving kinetically and spectrally overlapping intermediates of chromoproteins. *J. Phys. Chem. B 103*, 6371–6383.
44. Dickopf, S., and Heyn, M. P. (1997) Evidence for the first phase of the reorientation switch of bacteriorhodopsin from time-resolved photovoltage and flash photolysis experiments on the photoreversal of the M-intermediate. *Biophys. J. 73*, 3171–3181.
45. Joshi, C. P., Borucki, B., Otto, H., Meyer, T. E., Cusanovich, M. A., and Heyn, M. P. (2005) Photoreversal kinetics of the I_1 and I_2 intermediates in the photocycle of photoactive yellow protein by double flash experiments with variable time delay. *Biochemistry 44*, 656–665.
46. Borucki, B., Otto, H., Rottwinkel, G., Hughes, J., Heyn, M. P., and Lamparter, T. (2003) Mechanism of Cph1 phytochrome assembly from stopped-flow kinetics and circular dichroism. *Biochemistry 42*, 13684–13697.
47. Henry, E. R., and Hofrichter, J. (1992) Singular value decomposition: Application to analysis of experimental data. *Methods Enzymol. 210*, 129–192.
48. Otto, H., Hoersch, D., Meyer, T. E., Cusanovich, M. A., and Heyn, M. P. (2005) Time-resolved single tryptophan fluorescence in photoactive yellow protein monitors changes in the chromophore structure during the photocycle via energy transfer. *Biochemistry 44*, 16804–16816.
49. Unno, M., Kumauchi, M., Tokunaga, F., and Yamauchi, S. (2007) Vibrational assignment of the 4-hydroxycinnamoyl chromophore in photoactive yellow protein. *J. Phys. Chem. B 111*, 2719–2726.
50. Haker, A., Hendriks, J., van Stokkum, I. H., Heberle, J., Hellingwerf, K. J., Crielaard, W., and Gensch, T. (2003) The two photocycles of photoactive yellow protein from *Rhodobacter sphaeroides*. *J. Biol. Chem. 278*, 8442–8451.
51. Nie, B., Stutzman, J., and Xie, A. (2005) A vibrational spectral marker for probing the hydrogen-bonding status of protonated Asp and Glu residues. *Biophys. J. 88*, 2833–2847.
52. Chattoraj, M., King, B. A., Bublitz, G. U., and Boxer, S. G. (1996) Ultra-fast excited state dynamics in green fluorescent protein: multiple states and proton transfer. *Proc. Natl. Acad. Sci. U.S.A. 93*, 8362–8367.
53. Stoner-Ma, D., Jaye, A. A., Matousek, P., Towrie, M., Meech, S. R., and Tonge, P. J. (2005) Observation of excited-state proton transfer in green fluorescent protein using ultrafast vibrational spectroscopy. *J. Am. Chem. Soc. 127*, 2864–2865.
54. Hoersch, D., Otto, H., Cusanovich, M. A., and Heyn, M. P. (2009) Time-resolved spectroscopy of dye-labeled photoactive yellow protein suggests a pathway of light-induced structural changes in the N-terminal cap. *Phys. Chem. Chem. Phys. 11*, 5437–5444.
55. Imamoto, Y., Kataoka, M., and Tokunaga, F. (1996) Photoreaction cycle of photoactive yellow protein from *Ectothiorhodospira halophila* studied by low-temperature spectroscopy. *Biochemistry 35*, 14047–14053.
56. Shimizu, N., Imamoto, Y., Harigai, M., Kamikubo, H., Yamazaki, Y., and Kataoka, M. (2006) pH-dependent equilibrium between long lived near-UV intermediates of photoactive yellow protein. *J. Biol. Chem. 281*, 4318–4325.